Self Assembly

Reversible Self-Assembly of Nucleic Acids in a Diffusiophoretic Trap

Florian Katzmeier and Friedrich C. Simmel*

Abstract: The formation and dissociation of duplexes or higher order structures from nucleic acid strands is a fundamental process with widespread applications in biochemistry and nanotechnology. Here, we introduce a simple experimental system—a diffusiophoretic trap—for the non-equilibrium self-assembly of nucleic acid structures that uses an electrolyte gradient as the driving force. DNA strands can be concentrated up to hundred-fold by a diffusiophoretic trapping force that is caused by the electric field generated by the electrolyte gradient. We present a simple equation for the field to guide selection of appropriate trapping electrolytes. Experiments with carboxylated silica particles demonstrate that the diffusiophoretic force is long-ranged, extending over hundreds of micrometers. As an application, we explore the reversible self-assembly of branched DNA nanostructures in the trap into a macroscopic gel. The structures assemble in the presence of an electrolyte gradient, and disassemble upon its removal, representing a prototypical adaptive response to a macroscopic non-equilibrium state.

Introduction

Living organisms operate far from equilibrium, continuously dissipating energy to maintain their complex organization and structure. Concentration gradients commonly contribute to this process, serving as both energy sources and spatiotemporal organizers.[1] For instance, morphogen gradients trigger cell differentiation, chemical gradients direct chemotactic cellular movement, and transmembrane proton gradients provide energy to ATP synthases in mitochondria and chloroplasts. In this work, we introduce an experimental system that sustains a macroscopic physical non-equilibrium state in the form of a concentration gradient that promotes the local self-assembly of DNA nanostructures into macroscopic gels. Specifically, we utilize an electrolyte gradient to

drive the local up-concentration of branched DNA nanostars[2–10] via diffusiophoresis. The DNA nanostars undergo local self-assembly into gels, facilitated by their increased concentration and a favorable local electrolyte concentration for DNA strand hybridization. The assembly process is reversible, with the gels disassembling upon the removal of the gradient and can thus be understood as an adaptive response to an externally controlled macroscopic non-equilibrium state.

Diffusiophoresis[11] refers to the directed migration of macromolecules or colloids in a concentration gradient. This mechanism has recently been the focus of intense research[12–22] and has been used to concentrate colloids[23–26] and macromolecules.[27–29] In particular, it has been found that DNA accumulates near the orifice of a microcapillary ejecting an electrolyte in a microfluidic setting.[27,28] In the case of electrolyte gradients, the primary driving force for diffusiophoresis is an electric field generated by the gradient itself. This electric field points along the gradient and acts on charged macromolecules like DNA through electrophoresis. Notably, the existence of such an electric field caused by an electrolyte gradient was theoretically described by Planck over a century ago.[30] Mechanistically, the electric field arises from an asymmetry in the diffusion coefficients of the ions that constitute the electrolyte. For instance, anions with higher diffusion coefficients than cations will diffuse down the concentration gradient more rapidly. Such differential diffusion results in charge separation, generating an electric field with more negative charges at the lower end of the gradient and more positive charges at the upper end. In electrochemical experiments, the potential drop associated with this electric field is referred to as the liquid junction potential.[31]

Results and Discussion

As schematically shown in Figure 1a, a diffusiophoretic trap can be easily realized by filling a glass pipette with a highly concentrated electrolyte and submerging it in deionized water. The glass pipette is fixated in a commercially available pipette holder and is connected to a constant pressure supply via tubing. Upon application of a slight positive pressure on the pipette, the electrolyte flows out of the pipette tip, creating a steep electrolyte gradient near the orifice. When DNA molecules are present in the surrounding solution, they undergo directed migration towards the tip via diffusiophoresis. Close to the tip, the hydrodynamic force generated by the outflowing fluid exceeds the diffusiophoretic force, preventing DNA from entering the tip. As a result, DNA accumulates in a region in front of the

[*] F. Katzmeier, Prof. Dr. F. C. Simmel
Technical University of Munich
Physics of Synthetic Biological Systems
Arcisstraße 21, 80333 München (Germany)
E-mail: simmel@tum.de

Angew. Chem. Int. Ed. **2024**, *63*, e202317118 (1 of 6)

© 2024 The Authors. Angewandte Chemie International Edition published by Wiley-VCH GmbH
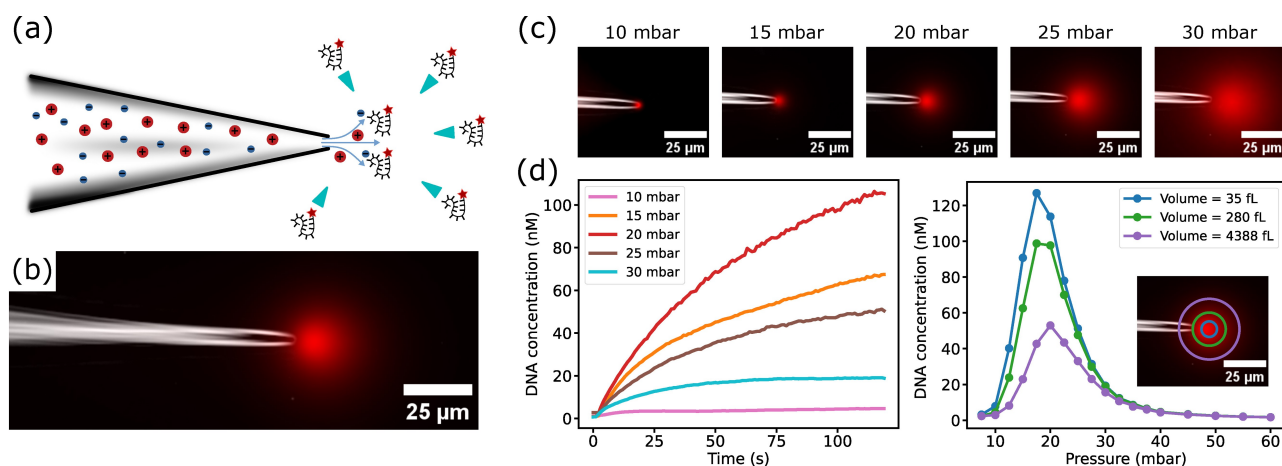
Figure 1. (a) Schematic representation of our experimental setup. A highly concentrated electrolyte, depicted with differently sized red and blue spheres to indicate ions with asymmetric diffusion constants, is ejected from a glass pipette to form an electrolyte gradient. Fluorescently labeled DNA strands are attracted through diffusiophoresis along the gradient towards the tip and accumulate there. The blue pointers indicate the direction of the diffusiophoretic force. (b) Overlay of an inverted brightfield image and a fluorescence image of the diffusiophoretic trap under operation. (c) Images of the diffusiophoretic trap 100 s after activation at different applied pressures. The brightness was individually adjusted in each image to ensure consistent visualization. (d) Left: Example time traces of the DNA concentration in a circular region of interest (ROI) around the trap, corresponding to a volume of approximately 280 fL. Right: DNA concentrations within the trap after 100 s for different pipette pressures, measured in the ROIs indicated in the inset.

tip where fluid flow and diffusiophoresis are balanced. In our experiments, we require an electric field such that negatively charged DNA migrates upwards along the electrolyte gradient toward the pipette tip. The electric field E in a two-component electrolyte gradient depends on the cation and anion diffusion coefficients D^+ and D^-, and their respective valencies z^+ and z^-:[13,32,33]

$$E \propto \frac{D^+ - D^-}{|z^+|D^+ + |z^-|D^-} \frac{\nabla c}{c} \tag{1}$$

Here, $\frac{\nabla c}{c}$ represents the normalized gradient of the electrolyte concentration c. An instructive derivation of this equation, along with an evolution equation for c, is given in the Supporting Information. Eq. (1) guides our selection of suitable electrolytes for diffusiophoretic trapping. As the direction of the electric field is determined by the difference of the diffusion coefficients $(D^+ - D^-)$, independent of ion valency, we require $D^+ < D^-$ for DNA trapping. Additionally, low-valency ions yield stronger electric fields, as z^+ and z^- only appear in the denominator. In our experiments, we use 200 mM Tris, titrated with HCl to pH 7.7, which primarily contains monovalent TrisH$^+$ ions with $D^+ = 0.8 \times 10^{-9}$ m^{2}s^{-1}[34] and Cl$^-$ ions with $D^- = 2.0 \times 10^{-9}$ m^{2}s^{-1} at $T = 298$ K. We also supplement the solution with 1 mM MgCl$_2$ to facilitate nucleic acid hybridization. Importantly, the diffusion coefficient of Mg^{2+} is 0.7×10^{-9} m^{2}s^{-1},[31] which also satisfies our criterion when compared to the diffusion coefficient of Cl$^-$. We hypothesize that combinations of such electrolytes should also be effective.

In initial experiments, we characterized the trap with 33 nucleotide (nt) long single-stranded DNA molecules ($c = 1$ nM) modified with a fluorescent dye. Figure 1b displays the trap 100 s after activation, showing a diffuse cloud of
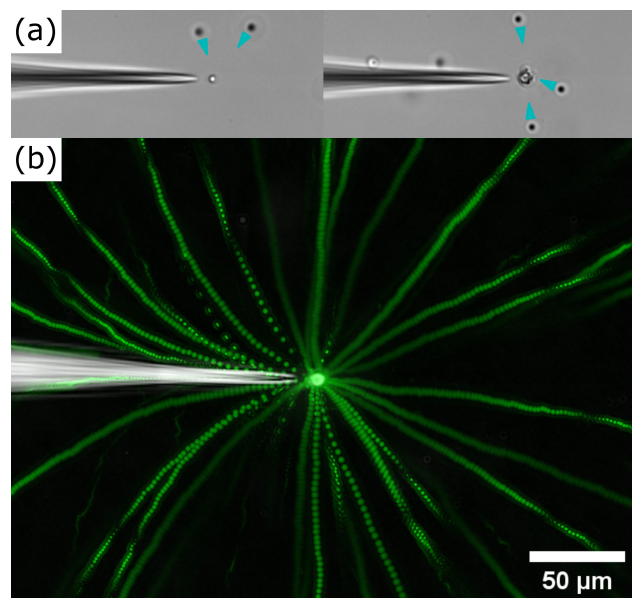
fluorescent DNA in front of the pipette tip. The fluorescent cloud forms directly after activation of the trap and grows in intensity until it reaches a steady state. We observed variations in the shape and intensity of the DNA cloud depending on the applied pipette pressure, as illustrated in Figure 1c. Low pressures lead to a more localized DNA accumulation, while high pressures result in a larger, more diffuse cloud. These variations in the extension of the accumulation region are not unexpected: higher pressures result in higher electrolyte efflux rates, altering the shape of the concentration gradient, and DNA accumulates in a region where the diffusiophoretic force balances the fluid flow, which changes depending on both the flow magnitude and the gradient shape.

We recorded microscopy videos to quantify the formation and growth of the trapped DNA cloud at varying pipette pressures. For data analysis, we defined a circular region of interest (ROI) around the cloud and measured its average fluorescence. The ROI is identified by finding the maximum intensity among all possible circular regions of the same size within an image. We then compared the region's average fluorescence to bulk fluorescence values for the same DNA strands at different concentrations, which allowed us to estimate the local DNA concentration within the trap. Figure 1d (left) displays example time traces which show the change in DNA concentration within a circular ROI with a volume of ≈ 280 fL. We observe up to a 100-fold increase in concentration within the trap, raising the DNA concentration from its bulk value of 1 nM to 100 nM. Further, we find that the concentration reaches a steady state after approximately 100 s. Notably, a pressure difference of 20 mbar results in more efficient up-concentration compared to lower (e.g., 10 mbar, 15 mbar) or higher (e.g.,

25 mbar, 30 mbar) pipette pressures, suggesting an optimal pressure condition.

We further quantified DNA trapping by measuring the DNA concentration within three differently sized ROIs after 100 s. The resulting data, showing DNA concentration as a function of pressure, are displayed in Figure 1d (right). For all three regions, we observe a peak trapping efficiency around 20 mbar. Additionally, we identify a minimum operational pressure difference of 10 mbar at which the trap becomes effective. At pressures exceeding 30 mbar, trapping efficiency becomes comparably low. Notably, the concentration peak shifts to slightly lower pressures for smaller regions of interest, consistent with our previous observation that lower pressures result in more localized DNA clouds.

To visualize the range of the diffusiophoretic force generated by the trap, we used carboxylated silica particles ($d = 2.1$ μm), which carry a negative charge and are therefore expected to migrate in the same direction as DNA in the trapping field. Operating the trap at 25 mbar, we observed accumulation of colloids in a region directly in front of the trap, as shown in Figure 2a. We also recorded a microscopy video of the colloid trapping process (Supporting Video 1), from which we generated an overlay image of the particle traces (Figure 2b) (details on video analysis are given in the Supporting Information). Our observations suggest that the diffusiophoretic trapping force is long-range, extending over hundreds of micrometers. This may seem surprising, as electric forces in electrolytes typically have a range defined by the Debye length, i.e., usually on the order of nanometers. However, in non-equilibrium 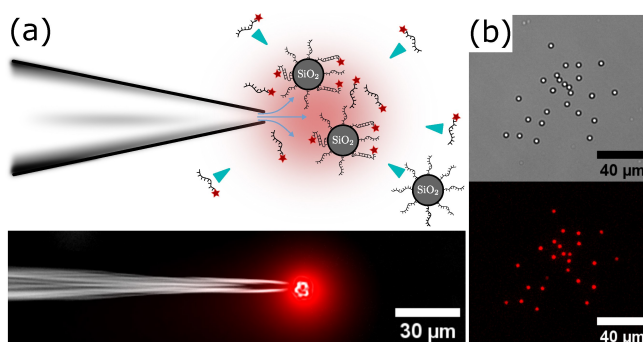scenarios, such as when a current is applied or, as in our case, when a concentration gradient is present, the electric force can extend over a much longer range. It is worth noting that, according to Eq. (1), the range of the diffusiophoretic force should in fact be similar to that of the concentration gradient.

Next, we investigated the diffusiophoretic trap's capacity to promote DNA hybridization reactions. Notably, the trap generates favorable conditions for such reactions in two respects: the trap locally enhances the DNA concentration by hundredfold, and the steep electrolyte gradient provides a high ionic strength within the trap. By contrast, in regions remote from the trap, both DNA and electrolyte concentrations are low, preventing DNA hybridization to occur.

Since both carboxylated silica particles and DNA accumulate in the trap, we studied hybridization reactions on the surface of the colloids, which can be easily monitored by microscopy. We modified the microparticles by activating their carboxyl groups with 1-Ethyl-3-(3-dimethyl-amino-propyl)-carbodiimide (EDC) and coupling them to 60 nt long amino-modified DNA capture strands.[35,36] We then operated the trap at 25 mbar using the DNA-modified colloids and a 5 nM solution of fluorescently labeled 30 nt long DNA strands, which had a sequence complementary to a subsequence of the DNA on the colloids (cf. Supporting Information). Both colloids and free DNA accumulate in the trap, allowing the free DNA to hybridize with the DNA on the colloids (Figure 3a). After 5 min of operation we turned off the trap and the colloids sedimented. The localization of fluorescence signal on the microparticles, which is visible in the fluorescence image of the sedimented colloids (Figure 3b), indicates successful DNA hybridization. We observed fluorescence on the particles for an additional 2 h, indicating that the fluorescent DNA was indeed stably bound to the capture strands. The complete experiment is documented in Supporting Video 2.

Lastly, we studied whether the diffusiophoretic trap can promote the assembly of branched DNA junctions—also termed Y-DNA[2,3,7] or DNA nanostars[4–6,8–10]—into macroscopic gels (cf. Figure 4a). Three-arm DNA nanostars are

Figure 2. (a) Microscopy images showing the trap operating in the presence of colloidal particles ($d = 2.1$ μm). The microparticles accumulate in front of the tip, their direction of movement is indicated with blue pointers. (b) Overlay image from a video (Supporting Video 1) that captures the attraction and accumulation of the microparticles. Particle traces are represented as green lines.

Figure 3. (a) DNA-modified silica particles and complementary strands are both accumulated in the diffusiophoretic trap. The locally high DNA and electrolyte concentrations promote DNA hybridization on the colloid surface. The blue pointers indicate the direction of the diffusiophoretic force. (b) Brightfield and fluorescence images of the sedimented particles after the trap was turned off (see also Supporting Video 2).
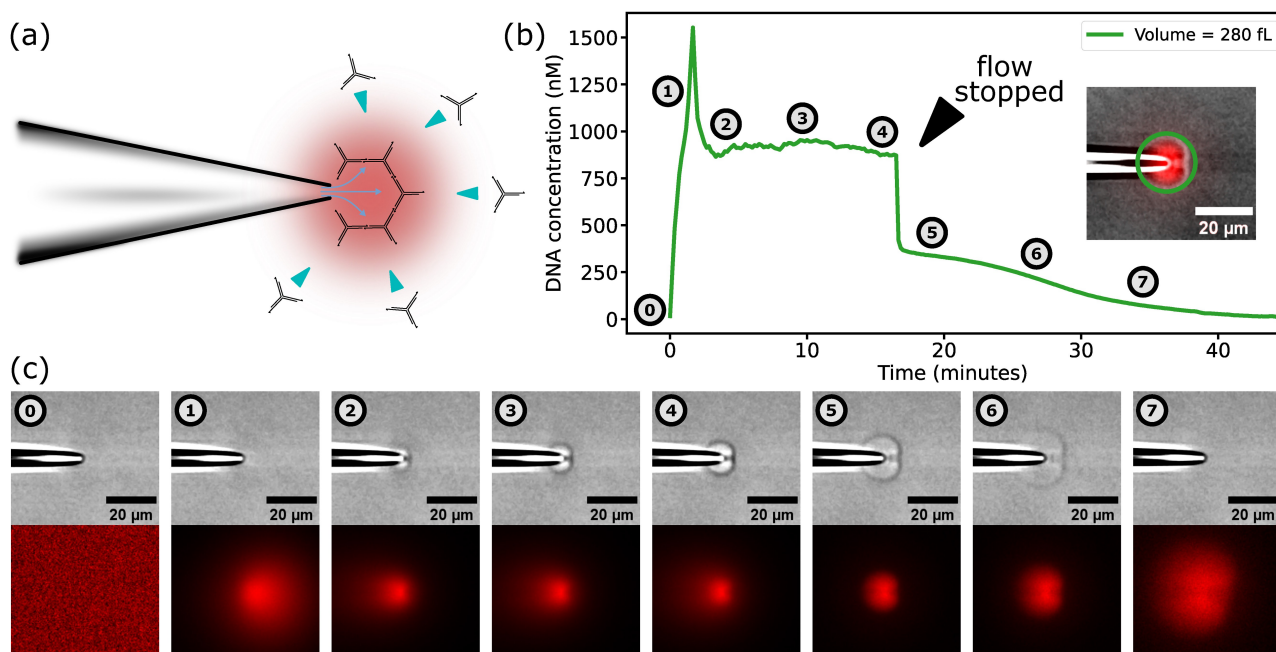
Figure 4. (a) Sketch illustrating how DNA nanostars are attracted and accumulate in a diffusiophoretic trap. The nanostars have selfcomplementary single-stranded overhangs that allow them to polymerize into a gel. (b) DNA concentration within a circular ROI close to the tip's pore during a DNA nanostar polymerization experiment. The ROI is shown in the microscopy image in the inset, numbers on the graph correspond to the images displayed in (c). (c) Brightfield and fluorescence images from selected frames of the nanostar polymerization experiment. The fluorescence intensity was individually adjusted for each frame.

composed of three 42 nt long single strands that hybridize together to form a Y-shaped nanostructure with three ≈7 nm long arms. Each arm of a nanostar features a single-stranded sticky end with a distinct self-complementary sequence, enabling the edges of the junctions to bind to each other and polymerize into a gel. We operated the diffusiophoretic trap with 5 nM DNA complexes. In order to be able to monitor their assembly via fluorescence micro-scopy, we substituted 1 nM of one of their constituent strands with a 33 nt long strand carrying a Cy5-label instead of the sticky end.

In Figure 4c, we show selected frames extracted from a microscopy video (Supporting Video 3) of the trap operating in the presence of nanostars. The video is further analyzed by plotting the fluorescence intensity within a circular region of interest as indicated in Figure 4b. Within roughly the first minute of operation (until time point 1), the fluorescence rapidly increases, corresponding to the formation of a diffuse DNA cloud similar as in the experiments shown in Figure 1. Between time points 1 and 2, the shape of the fluorescent cloud changes and its intensity drops. Simulta-neously, in the brightfield image a distinct structure appears in front of the tip, which we interpret as the formation of a DNA gel. The change in shape of the fluorescent cloud is likely due to the altered hydrodynamic flow and electrolyte gradient caused by the presence of the DNA gel. The gel continues to grow in size between time points 2 and 4, while maintaining a relatively constant fluorescence level. After 17 minutes (between time points 4 and 5), we stopped the electrolyte flow, eliminating the gradient and thus terminat-

ing the trapping process. We observed a quick initial expansion in the size of the gel, accompanied by a rapid decrease in fluorescence. The gel continues to expand until it is no longer visible in either the fluorescence or brightfield channels. We repeated the DNA gel formation experiment multiple times and found similar behavior as in Figure 4b in each case (see Supporting Information).

The observed behavior can be explained with the viscoelastic properties of DNA nanostar gels.[4,6,7] The rapid expansion of the gel following trap deactivation is a consequence of the elasticity of the DNA gel. During operation of the trap, the gel is compressed by the force exerted through the electric field. Upon removal of this force, the gel quickly relaxes and expands. The swift decrease in fluorescence after time point 4 can be attributed to the diffusion of unbound DNA molecules out of the trap. The later phase of the dissolution process (time points 6 and 7) is characterized by a slow expansion of the gel and fading visibility, indicating swelling and bulk erosion. As the gel forms under a compressive force and at high DNA concentrations, it initially comprises a densely intercon-nected matrix. During dissolution, nanostars dissociate with-in the gel and either escape or bind elsewhere. This results in a reduced crosslinking density, leading to elastic relaxa-tion and expansion of the gel matrix.

Finally, we wish to discuss the physical non-equilibrium state of the DNA during the trapping process. While it seems intuitive to describe the trapping mechanism as DNA accumulation in a potential well created by the interplay of the electric field and hydrodynamic flow, this notion is not

entirely accurate. A stationary state, resulting from a balance between electric and hydrodynamic forces, cannot be described as an equilibration process in an energy minimum. Typically, the hydrodynamic flow field cannot be expressed as a gradient field, and consequently, the resultant hydrodynamic force cannot be either. Therefore, we anticipate that DNA continues to be actively transported within the system, even when it reaches a steady state. In simpler terms, the mass flux of the DNA may remain non-zero even at steady state, indicating that the accumulation is more akin to a traffic jam than a static collection. Regarding the assembly of DNA gels, the trap creates locally favorable conditions, specifically high concentrations of nanostars and electrolytes, accompanied by a continuous supply of new material for the sustained growth of the gel.

Conclusion

In conclusion, we have developed a diffusiophoretic trap capable of locally concentrating both DNA and colloids, as well as promoting hybridization between complementary DNA strands. Moreover, we explored the reversible self-assembly of DNA nanostars into macroscopic structures. An electric field, generated by an electrolyte gradient, serves as the driving force for assembly, accumulating the DNA and creating favorable conditions for strand hybridization. When the gradient is removed, along with the localization force and favorable hybridization conditions, the gel gradually disassembles.

In addition to its fundamental scientific interest as a non-equilibrium dynamical system, the diffusiophoretic trap has potential technological applications. Our experiments demonstrate that the trap can concentrate charged colloids or molecules. This method could be utilized to extract these substances from diluted environmental samples, preconcentrate them prior to analysis,[27] or select and sort them based on charge. Furthermore, the local up-concentration mechanism provides a possibility to speed up concentration-dependent reactions, which might prove useful for the development of low cost DNA or RNA detection systems.

Lastly, we wish to highlight other physical non-equilibrium systems that similarly promote local up-concentration and interactions among nucleic acids. Most notably, temperature gradients are known to locally trap DNA via thermophoresis, under specific conditions.[37–39] Thermal gradients have even have been observed to drive the gelation of nucleic acids.[40] Additionally, two other non-equilibrium settings, wet-dry cycles[41–45] and freeze-thaw cycles,[46–48] are noteworthy as they exhibit effects similar to those observed in our diffusiophoretic trap. Freezing and evaporation effectively reduce the reaction volume, leading to locally high concentrations of electrolytes and reactants, which in turn enhances the efficiency of biochemical reactions.

Naturally, these mechanisms have also been investigated as solutions to the concentration problem in prebiotic evolution scenarios, where achieving sufficiently high concentrations of organic molecules in dilute primordial environments is crucial for the reactions leading to the formation of the first biomolecules.[49] Notably, pH gradients[24,50] and concentration gradients,[51] emulating hydrothermal vent conditions, have been explored in this context.

In principle, electrolyte gradients can occur in similar settings, e.g., in porous rocks that leach dissolving salts or in saltwater springs. According to Eq. (1), salts suitable for the diffusiophoretic trapping of nucleic acids comprise most halogen salts of divalent or trivalent metal ions.[31] Alkaline solutions are also expected to be effective, due to the exceptionally high diffusion constant of OH^-. Notably, calcium carbonate, a commonly occurring mineral, has previously been demonstrated to be effective in driving diffusiophoresis.[13] However, we have to acknowledge that our diffusiophoretic trap operates within a relatively narrow range of parameters, as evidenced by the optimal pressure range deduced in Figure 1. Critical factors, including pore size, outflow rate, and the electrolyte composition inside and outside, require precise calibration, suggesting that the effect may not be very common in natural environments.

Conflict of Interest

The authors declare no conflict of interest.

Data Availability Statement

The data that support the findings of this study are available from the corresponding author upon reasonable request.

[1] R. Phillips, J. Kondev, J. Theriot, H. Garcia, *Physical Biology of the Cell*, Garland Science, 2nd ed. edition **2012**.

[2] Y. Li, Y. D. Tseng, S. Y. Kwon, L. d'Espaux, J. S. Bunch, P. L. McEuen, D. Luo, *Nat. Mater.* **2004**, *3*, 38.

[3] S. H. Um, J. B. Lee, N. Park, S. Y. Kwon, C. C. Umbach, D. Luo, *Nat. Mater.* **2006**, *5*, 797 .

[4] S. Biffi, R. Cerbino, F. Bomboi, E. M. Paraboschi, R. Asselta, F. Sciortino, T. Bellini, *Proc. Natl. Acad. Sci. USA* **2013**, *110*, 15633.

[5] L. Rovigatti, F. Smallenburg, F. Romano, F. Sciortino, *ACS Nano* **2014**, *8*, 3567.

[6] G. Nava, M. Rossi, S. Biffi, F. Sciortino, T. Bellini, *Phys. Rev. Lett.* **2017**, *119*, 078002.

[7] Z. Xing, A. Caciagli, T. Cao, I. Stoev, M. Zupkauskas, T. O'Neill, T. Wenzel, R. Lamboll, D. Liu, E. Eiser, *Proc. Natl. Acad. Sci. USA* **2018**, *115*, 8137.

[8] R. A. Brady, W. T. Kaufhold, N. J. Brooks, V. Foderà, L. D. Michele, *J. Phys. Condens. Matter* **2019**, *31*, 074003.

[9] Y. Sato, T. Sakamoto, M. Takinoue, *Sci. Adv.* **2020**, *6*, eaba3471.

[10] S. Agarwal, D. Osmanovic, M. A. Klocke, E. Franco, *ACS Nano* **2022**, *16*, 11842.

[11] J. L. Anderson, D. C. Prieve, *Sep. Purif. Methods* **1984**, *13*, 67.

[12] J. J. McDermott, A. Kar, M. Daher, S. Klara, G. Wang, A. Sen, D. Velegol, *Langmuir* **2012**, *28*, 15491.

[13] T.-Y. Chiang, D. Velegol, *J. Colloid Interface Sci.* **2014**, *424*, 120.

[14] J. S. Paustian, C. D. Angulo, R. Nery-Azevedo, N. Shi, A. I. Abdel-Fattah, T. M. Squires, *Langmuir* **2015**, *31*, 4402.

[15] A. Kar, T.-Y. Chiang, I. Ortiz Rivera, A. Sen, D. Velegol, *ACS Nano* **2015**, *9*, 746.

[16] A. Banerjee, I. Williams, R. N. Azevedo, M. E. Helgeson, T. M. Squires, *Proc. Natl. Acad. Sci. USA* **2016**, *113*, 8612.

[17] S. Shin, E. Um, B. Sabass, J. T. Ault, M. Rahimi, P. B. Warren, H. A. Stone, *Proc. Natl. Acad. Sci. USA* **2016**, *113*, 257.

[18] D. Velegol, A. Garg, R. Guha, A. Kar, M. Kumar, *Soft Matter* **2016**, *12*, 4686.

[19] A. Gupta, S. Shim, H. A. Stone, *Soft Matter* **2020**, *16*, 6975.

[20] B. Ramm, A. Goychuk, A. Khmelinskaia, P. Blumhardt, H. Eto, K. A. Ganzinger, E. Frey, P. Schwille, *Nat. Phys.* **2021**, *17*, 850.

[21] S. Shim, *Chem. Rev.* **2022**, *122*, 6986.

[22] Q. A. E. Peter, R. P. B. Jacquat, T. W. Herling, P. K. Challa, T. Kartanas, T. P. J. Knowles, *J. Phys. Chem. B* **2022**, *126*, 8913.

[23] B. Abécassis, C. Cottin-Bizonne, C. Ybert, A. Ajdari, L. Bocquet, *Nat. Mater.* **2008**, *7*, 785.

[24] F. M. Möller, F. Kriegel, M. Kieß, V. Sojo, D. Braun, *Angew. Chem. Int. Ed.* **2017**, *56*, 2340.

[25] J. Palacci, B. Abécassis, C. Cottin-Bizonne, C. Ybert, L. Bocquet, *Phys. Rev. Lett.* **2010**, *104*, 138302.

[26] N. Shi, R. Nery-Azevedo, A. I. Abdel-Fattah, T. M. Squires, *Phys. Rev. Lett.* **2016**, *117*, 258001.

[27] S. M. Friedrich, J. M. Burke, K. J. Liu, C. F. Ivory, T.-H. Wang, *Nat. Commun.* **2017**, *8*, 1213.

[28] S. Li, A. Li, K. Hsieh, S. M. Friedrich, T.-H. Wang, *Anal. Chem.* **2020**, *92*, 6150.

[29] M. K. Rasmussen, J. N. Pedersen, R. Marie, *Nat. Commun.* **2020**, *11*, 2337.

[30] M. Planck, *Ann. Phys.* **1890**, *276*, 561.

[31] P. H. Barry, J. W. Lynch, *J. Membr. Biol.* **1991**, *121*, 101.

[32] A. Gupta, B. Rallabandi, H. A. Stone, *Phys. Rev. Fluids* **2019**, *4*, 043702.

[33] J. L. Wilson, S. Shim, Y. E. Yu, A. Gupta, H. A. Stone, *Langmuir* **2020**, *36*, 7014.

[34] B. Ng, P. H. Barry, *J. Neurosci. Methods* **1995**, *56*, 37.

[35] N. Nakajima, Y. Ikada, *Bioconjugate Chem.* **1995**, *6*, 123.

[36] D. Sehgal, I. K. Vijay, *Anal. Biochem.* **1994**, *218*, 87.

[37] C. B. Mast, D. Braun, *Phys. Rev. Lett.* **2010**, *104*, 188102.

[38] M. Kreysing, L. Keil, S. Lanzmich, D. Braun, *Nat. Chem.* **2015**, *7*, 203.

[39] A. Salditt, L. M. R. Keil, D. P. Horning, C. B. Mast, G. F. Joyce, D. Braun, *Phys. Rev. Lett.* **2020**, *125*, 048104.

[40] M. Morasch, D. Braun, C. B. Mast, *Angew. Chem. Int. Ed.* **2016**, *55*, 6676.

[41] S. Rajamani, A. Vlassov, S. Benner, A. Coombs, F. Olasagasti, D. Deamer, *Origins Life Evol. Biospheres* **2008**, *38*, 57.

[42] S. Becker, C. Schneider, H. Okamura, A. Crisp, T. Amatov, M. Dejmek, T. Carell, *Nat. Commun.* **2018**, *9*, 163.

[43] L. Da Silva, M.-C. Maurel, D. Deamer, *J. Mol. Evol.* **2015**, *80*, 86.

[44] A. V. Dass, S. Wunnava, J. Langlais, B. von der Esch, M. Krusche, L. Ufer, N. Chrisam, R. C. A. Dubini, F. Gartner, S. Angerpointner, C. F. Dirscherl, P. Rovó, C. B. Mast, J. E. Šponer, C. Ochsenfeld, E. Frey, D. Braun, *ChemSystemsChem* **2023**, *5*, e202200026.

[45] S. Dagar, S. Sarkar, S. Rajamani, *Origins Life Evol. Biospheres* **2023**, *53*, 43.

[46] J. Attwater, A. Wochner, V. B. Pinheiro, A. Coulson, P. Holliger, *Nat. Commun.* **2010**, *1*, 76.

[47] H. Mutschler, A. Wochner, P. Holliger, *Nat. Chem.* **2015**, *7*, 502.

[48] S. J. Zhang, D. Duzdevich, D. Ding, J. W. Szostak, *Proc. Natl. Acad. Sci. USA* **2022**, *119*, e2116429119.

[49] A. Ianeselli, A. Salditt, C. Mast, B. Ercolano, C. L. Kufner, B. Scheu, D. Braun, *Nat. Rev. Phys.* **2023**, *5*, 185.

[50] V. Helmbrecht, M. Weingart, F. Klein, D. Braun, W. D. Orsi, *Geobiology* **2023**, *21*, 758.

[51] T. Matreux, K. Le Vay, A. Schmid, P. Aikkila, L. Belohlavek, A. Z. Çalışkanoğlu, E. Salibi, A. Kühnlein, C. Springsklee, B. Scheu, D. B. Dingwell, D. Braun, H. Mutschler, C. B. Mast, *Nat. Chem.* **2021**, *13*, 1038.